Journal of Power Sources 196 (2011) 9204–9212

Contents lists available at ScienceDirect

Journal of Power Sources

journal homepage: www.elsevier.com/locate/jpowsour

Effect of stress on dissolution/precipitation of platinum: Implications concerning core–shell catalysts and cathode degradation in proton exchange membrane fuel cells

Preethy Parthasarathy, Anil V. Virkar*

Department of Materials Science & Engineering, University of Utah, 122 S. Central Campus Drive, Salt Lake City, UT 84112, USA

ARTICLE INFO

Article history:
Received 24 May 2011
Received in revised form 6 July 2011
Accepted 7 July 2011
Available online 19 July 2011

Keywords:
Platinum
Dissolution
Catalyst
Stress
Fuel cells

ABSTRACT

Effect of applied stress on dissolution/precipitation of platinum was investigated. Two platinum wires/foils were partially immersed in a $PtCl_4$ solution in DMSO. A tensile load was applied to one wire/foil and the other one was left load free. The wire/foil subjected to a tensile load developed a positive potential (became cathodic) with respect to the unstressed wire/foil. This observation suggests that under a tensile stress, the chemical potential of Pt decreases. This result suggests design strategies for core–shell catalysts used in proton exchange membrane fuel cells (PEMFCs). Nanosize catalyst particles are under compression due to the Gibbs–Thompson effect. Core–shell catalysts have additional stresses in the shell depending upon lattice parameters of the core and the shell. The present results suggest that stable core–shell catalysts for PEMFC with Pt shell should be designed such that the shell is under a tensile stress (or reduced compression compared to monolithic catalyst particles). The present results also suggest that from the standpoint of stability, the lattice parameter of the core should be larger than that of the shell.

1. Introduction

Proton exchange membrane fuel cells (PEMFCs) are electrochemical devices which convert chemical energy of oxidation of hydrogen into electrical energy. Typical PEMFC consist of a polymeric proton exchange membrane (e.g. Nafion) as the electrolyte sandwiched between a cathode and an anode. Considerable work has been reported on PEMFC over the past two decades. Proton exchange membrane fuel cells (PEMFCs) have applications in transportation, distributed power, and portable power. In automotive applications, PEMFC have shown considerable promise with several pilot vehicles having demonstrated cumulatively hundreds of thousands of road miles. In portable power, excellent performance has also been shown on liquid fuels, especially methanol.

While considerable progress has been made over the past two decades in PEMFC, it is well known that degradation in performance occurs over time. This degradation in performance has a direct bearing on the ultimate cost of PEMFC, and has in part limited the commercial exploitation of PEMFC on a large scale. There are many factors which influence PEMFC degradation. These include the materials used in PEMFC and the operating conditions. Typically, both the cathode and the anode of a PEMFC contain nanosize noble metal (Pt) or noble metal alloy particles supported on high surface area carbon. One of the reasons for alloying Pt with non-noble metals is to reduce the Pt loading and thus lower the cost [1–8]. The lowering of Pt loading can also be achieved by making core–shell catalysts with core made of a non-noble metal or a Pt alloyed with a non-noble metal and a shell of Pt. Considerable work has been reported on core–shell catalysts [9–34].

Several mechanisms of cathode degradation have been reported [35–46]. They include: (a) detachment of catalyst particles from carbon support thus rendering them electro-catalytically inactive. (b) Ostwald ripening of particles. (c) Agglomeration and associated growth (sintering) of particles. (d) Dissolution of the catalyst at the cathode, its transport and precipitation into the membrane. All of these phenomena lead to a decrease in the catalyst surface area, decrease in catalytic activity, and thus loss in performance. Insofar as the operating conditions are concerned, studies have shown that greater degradation occurs at open circuit than when the fuel cell is under load. This observation has important implications concerning the idling characteristics of a PEMFC. It is also known that negligible degradation occurs at the anode even when its composition is substantially the same as the cathode.

Ostwald ripening, agglomeration and sintering, and precipitation in the membrane all depend upon some aspects of local dissolution of Pt, its transport, and its precipitation [47]. The ther-

* Corresponding author. Tel.: +1 801 581 5396; fax: +1 801 581 4816.
E-mail address: anil.virkar@m.cc.utah.edu (A.V. Virkar).

0378-7753/$ – see front matter © 2011 Elsevier B.V. All rights reserved.
doi:10.1016/j.jpowsour.2011.07.027

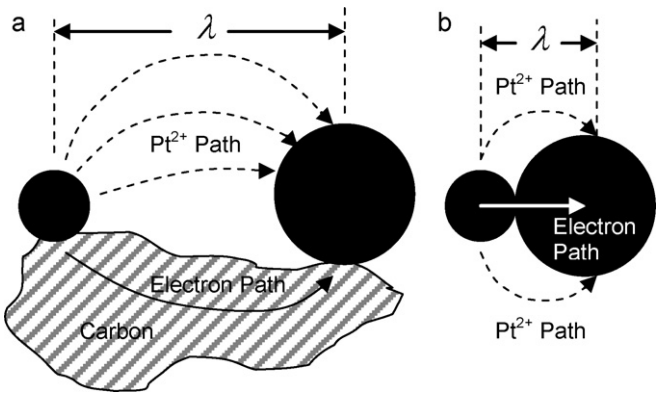

Fig. 1. Mechanism of particle growth by (a) Ostwald ripening and (b) agglomeration/sintering. Both occur by a coupled transport of Pt^{2+} (or Pt^{4+}) ions through ionomer/aqueous media and electron transport through the carbon support (or through direct particle to particle contact). Net Pt transport occurs from smaller particles to larger particles.

modynamic driving force for agglomeration/sintering and Ostwald ripening is the reduction in surface energy accompanying particle growth. This phenomenon leads to dissolution of smaller particles and growth of larger particles. Ostwald ripening occurs by the dissolution of particles into a medium, transport through the medium and deposition on larger particles. In PEMFC, transport of electrically neutral Pt occurs via a coupled process involving the transport of ions (Pt^{2+} and/or Pt^{4+}) through an ionomer/aqueous medium and a parallel (coupled) transport of electrons through the carbon support [48]. In agglomeration/sintering a similar process occurs where ions transport through ionomer/aqueous medium and electrons transport through a direct particle-to-particle contact. Fig. 1 shows schematics of the growth of Pt particles by dissolution/precipitation of isolated particles (supported on high surface area carbon) and of particles in direct physical contact with each other (agglomeration/sintering). The fundamental physical parameter which dictates degradation kinetics is the electrochemical potential of Pt ions, which depends upon the chemical potential of Pt. All those factors which lower the chemical potential of Pt should generally decrease the kinetics of degradation, and all those factors which increase the chemical potential of Pt should increase the kinetics of degradation.

The chemical potential of a species depends on composition, temperature and pressure. Alloying Pt with other metals lowers the chemical potential of Pt. Many alloys of Pt are currently being explored for application as PEMFC catalysts [1–8]. Hydrostatic stress (pressure) also affects the chemical potential. This of course is well known and is the basis of the Gibbs–Thompson equation and is the reason for the occurrence of Ostwald ripening/agglomeration [49]. The dependence of chemical potential of Pt, μ_{Pt}, on temperature, composition and pressure is given by [49]

$$\mu_{Pt} = \mu_{Pt}^{o} + RT \ \ln a_{Pt} + pV_m \quad (1)$$

where μ_{Pt}^{o} is the standard state chemical potential of Pt, a_{Pt} is the activity of Pt, V_m is the partial molar volume of Pt, and p is the pressure. If the material is pure Pt, then a_{Pt} is unity. For nanosize particles, the pressure is given by $2\gamma/r$, where r is the particle radius and γ is the surface energy. Thus, the smaller the particle size, the higher is the pressure inside the particle, the higher is the chemical potential, and the greater is the tendency for its dissolution and deposition on larger particles.

Eq. (1) is very general in that the sign of pressure determines whether it will increase or decrease the chemical potential. In a sample of any general geometric shape, (locally) positive or negative pressure can be created by the application of external forces. If the pressure is positive (compressive), the chemical potential will be higher compared to a stress-free material. If the pressure is negative (tensile), however, the chemical potential should be lower compared to a stress-free material. The effect of stress on electrode potentials of metals was investigated during the 1950s and 1960s, primarily to determine the effect of stress on corrosion. Several authors had assumed that the dominant stress-related term in chemical potential is the strain energy, which is proportional to the square of stress (or the square of pressure). The expectation under this assumption was that electrode potential should be the same in both tension and compression for a given magnitude of stress. However, many experimental results were found to be inconsistent with this expectation [50,51]. It was in fact observed that the sign of electrode potential depended upon whether the applied load was tensile or compressive [50,51]. Flood [52] in a classic paper demonstrated that the dominant term in chemical potential is in fact linearly related to pressure (consistent with Eq. (1)), and thus electrode potential is expected to exhibit a reversal in sign upon a reversal in the sign of stress (tensile or compressive), in accord with the general thermodynamic theory of Gibbs. This result is actually not surprising. Indeed, it is well known in theories of creep that matter movement occurs from regions of compression to regions of tension.

The analysis by Flood [52] has significant bearing on the role of stress on catalyst stability and specifically on the design of core–shell catalysts. Core–shell catalysts typically consist of a core and a shell of different materials but generally of the same crystal structure, and with an epitaxially matched interface. The lattice parameters of the core and the shell determine the magnitudes and the signs of the induced stresses in the shell and in the core of a core–shell catalyst. If the Pt shell is under greater compression than a pure Pt catalyst particle of the same diameter, the chemical potential of Pt will be higher in the shell of the core–shell catalyst than the monolithic Pt catalyst. Such a catalyst should exhibit increased tendency for dissolution. If the Pt shell is under reduced compression (or even possibly in tension) than a pure Pt catalyst of the same diameter, the chemical potential of Pt in the shell will be lower in the core–shell catalyst than in the monolithic Pt catalyst of the same diameter. Such a catalyst should exhibit decreased tendency for dissolution and thus should exhibit increased stability. An example is a core shell catalyst with Pt shell and Ag or Au core. Such core–shell catalysts should be inherently more stable compared to pure Pt catalysts of the same outer diameter.

The objective of the present work was to investigate the role of stress on the chemical potential of Pt using an electrochemical technique. This was achieved using Pt wires/foils of macroscopic dimensions as electrodes. Implications of the results for the design of core–shell catalysts for PEMFC are discussed. The implications for core–shell catalysts are further compared with some recent literature on atomistic level (DFT) calculations of core–shell catalysts.

2. Theory

Fig. 2 shows a schematic of the experimental set up used. Platinum (IV) chloride dissolved in DMSO was used as the electrolyte to investigate the effect of tensile stress on electrode potential. When Pt wire/foil is immersed in $PtCl_4$/DMSO solution the following chemical reaction (locally) is expected to take place

$$Pt + PtCl_4 \rightarrow 2PtCl_2 \quad (2)$$

since the standard Gibbs free energy change at room temperature for the above reaction is $-23.02\ kJ\ mol^{-1}$ [53]. The solubility of $PtCl_2$ in DMSO is very small. The electrolyte will thus mainly contain Pt^{4+} ions with a small concentration of Pt^{2+}. When a tensile load is applied to one of the wires/foils, the chemical potential of Pt in the stressed wire/foil will decrease and platinum ions will initially

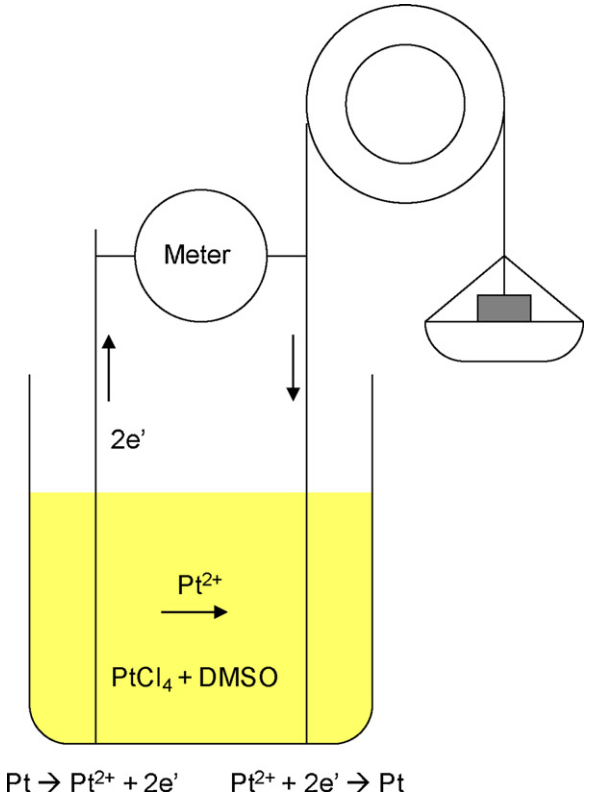

Fig. 2. A schematic of the experimental setup used. For the measurement of voltage difference, the meter used was a high impedance meter. For the measurement of current, the meter used was an ammeter.

transport from the unstressed platinum wire/foil to the stressed platinum wire/foil through the electrolyte. Negligible transport of electrons occurs under open circuit conditions since the *electronic* conductivity of the electrolyte is negligible. The transport of Pt^{2+} ions shuts down as soon as the electrochemical potentials of Pt^{2+} ions in both the stressed and the unstressed wires become equal, that is

$$\tilde{\mu}_{Pt^{2+}}^{\text{unstressed}} = \tilde{\mu}_{Pt^{2+}}^{\text{stressed}} \tag{3}$$

where $\tilde{\mu}_{Pt^{2+}} = \mu_{Pt^{2+}} + 2F\Phi$ is the electrochemical potential of Pt^{2+}, $\mu_{Pt^{2+}}$ is the chemical potential of Pt^{2+}, F is the Faraday constant, and Φ is the local electrostatic potential. Now, within platinum metal, the reaction $Pt \leftrightarrow Pt^{2+} + 2e'$ is at equilibrium. Thus,

$$\mu_{Pt} = \mu_{Pt^{2+}} + 2\mu_e = \tilde{\mu}_{Pt^{2+}} + 2\tilde{\mu}_e = \tilde{\mu}_{Pt^{2+}} - 2F\varphi \tag{4}$$

where

$$\varphi = -\frac{\tilde{\mu}_e}{F} = -\frac{\mu_e}{F} + \Phi \tag{5}$$

in which μ_e is the chemical potential of electrons, $\tilde{\mu}_e$ is the electrochemical potential of electrons, and φ is the experimentally measurable electric potential. Thus, the electrochemical potential of platinum ions in terms of the chemical potential of neutral Pt and the measurable electric potential is given by

$$\tilde{\mu}_{Pt^{2+}} = \mu_{Pt} - 2\tilde{\mu}_e = \mu_{Pt} + 2F\varphi \tag{6}$$

The electrochemical potentials of Pt^{2+} in the unstressed and the stressed Pt wires are given respectively by

$$\tilde{\mu}_{Pt^{2+}}^{\text{unstressed}} = \tilde{\mu}_{Pt}^{o} + 2F\varphi^{\text{unstressed}} \tag{7}$$

and

$$\tilde{\mu}_{Pt^{2+}}^{\text{stressed}} = \mu_{Pt}^{o} + pV_m + 2F\varphi^{\text{stressed}} = \mu_{Pt} + 2F\varphi^{\text{stressed}} \tag{8}$$

Substituting Eqs. (7) and (8) into Eq. (3) gives

$$2F(\varphi^{\text{stressed}} - \varphi^{\text{unstressed}}) = -pV_m = -(\mu_{Pt} - \mu_{Pt}^{o}) \tag{9}$$

and

$$(\varphi^{\text{stressed}} - \varphi^{\text{unstressed}}) = \Delta\varphi = -\frac{pV_m}{2F} = -\frac{\mu_{Pt} - \mu_{Pt}^{o}}{2F} \tag{10}$$

That is, when a tensile load is applied, the hydrostatic pressure will be negative which makes the stressed platinum wire positive (cathodic) – a sort of stress-induced cathodic protection. An important point to note is that Eq. (10) is independent of the nature of the anion (here Cl^-). The role of anion will be only in the kinetics of transport, but not in thermodynamics.

3. Experimental procedure

Fig. 2 shows the experimental setup used. Two identical platinum wires of diameter 127 μm were partially immersed in 0.1 M platinum chloride ($PtCl_4$)/DMSO solution. The distance between the two wires was set at 1 mm. A tensile load was applied to one of the platinum wires using a pan tied to it and the other one was maintained stress-free. The pan attached to the wire was passed over a pulley. The load on the stressed wire was varied by adding several standard weights to the pan. The corresponding stress was varied between ~0 MPa and ~210 MPa. Any voltage created between the wires was measured using an electrometer (Keithley 6514) with a high input impedance (200 TeraΩ). In another experiment an ammeter, capable of measuring current in the pA range, was connected between the two wires (effectively externally shorting the two wires) and the current passing through the external circuit was measured as a function of the applied mechanical load. The corresponding stress was varied between ~0 MPa and ~195 MPa. Yield stress of platinum is typically ~100–180 MPa. Thus, at the higher values of the applied stress, some deformation (and work-hardening) is expected. However, it is expected that upon work hardening, the yield stress would increase and the sample will be still in the elastic regime after the initial deformation. Similar experiments were also conducted using two identical platinum foils of thickness 127 μm and width 0.5 cm placed 1 mm apart, partially immersed in 0.1 M $PtCl_4$/DMSO solution. Voltage (open circuit) and current (short circuit) were measured as a function of the applied stress ranging between 0 and 9 MPa.

In order to investigate the effect of stress on the kinetics of transport of platinum between the unstressed and the stressed wires/foils over a period of time, the same setup was used as above. Two identical platinum wires were partially immersed in the $PtCl_4$ electrolyte solution separated by a distance of 1 mm. A constant tensile stress of 153 MPa was applied to one of the wires. The wires were electrically shorted externally to provide a path for electrons. The expectation was that platinum will dissolve at the unstressed wire and will deposit on the stressed wire. After 144 h, the platinum wires were cleaned and examined under a scanning electron microscope (SEM). A similar experiment was also conducted using platinum foils of thickness 127 μm and width 0.5 cm. A tensile stress of 4.5 MPa was applied for 144 h. The platinum foils were then cleaned and examined under an SEM.

Another set of experiments was conducted in which platinum wires ranging in diameters between 0.01 mm and 0.6 mm were used. In each experiment in this set, the two electrodes were of identical diameters. For a given wire diameter, the voltage between the stressed and the unstressed wires was measured as a function of the applied tensile stress. These experiments were conducted in order to determine the possible effect of the wire diameter on the dependence of voltage on the applied tensile stress.

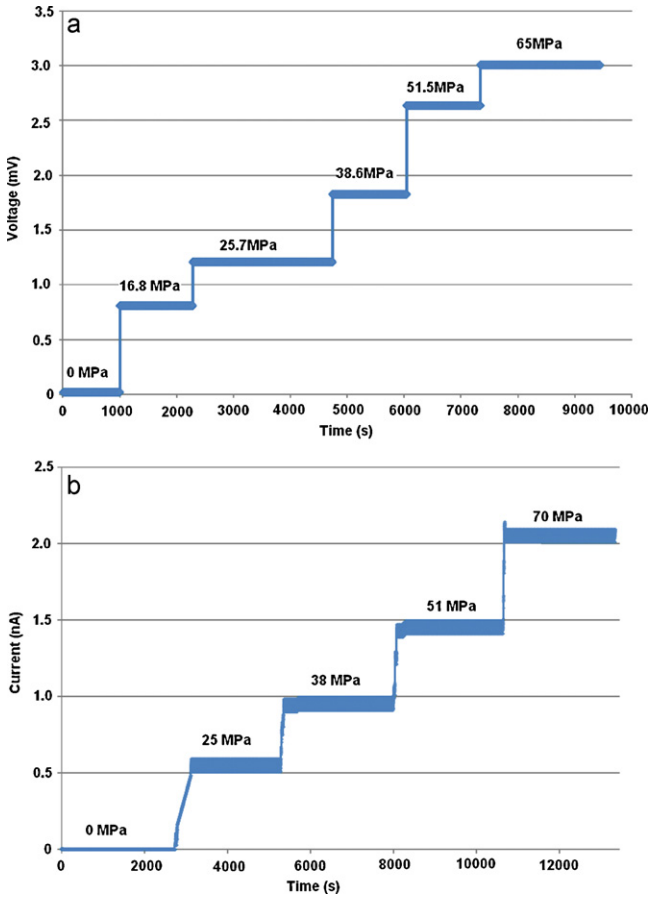

Fig. 3. (a) Variation of the voltage between the stressed (positive) and the unstressed Pt wires immersed in 0.1 M $PtCl_4$/DMSO solution for different applied loads. (b) Variation of the current between the stressed and the unstressed platinum wires immersed in 0.1 M $PtCl_4$/DMSO solution for different applied loads.

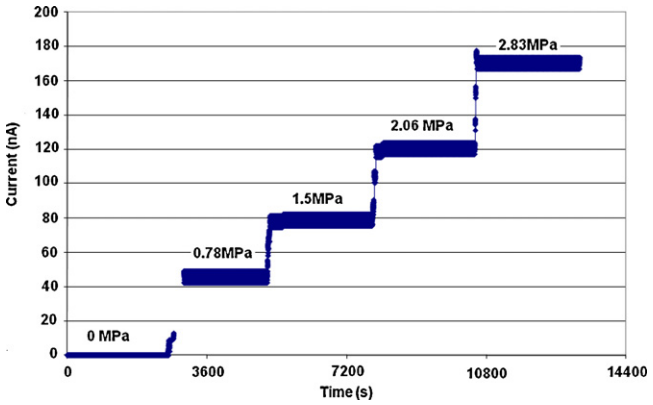

Fig. 4. Variation of the current between the stressed and the unstressed Pt foils immersed in 0.1 M $PtCl_4$/DMSO solution for different applied loads.

4. Results and discussion

4.1. Effect of stress on electrode potential

Fig. 3(a) and (b) shows voltage (open circuit) and current (short circuit) vs. time plots for the experiments conducted on platinum wires under various applied tensile loads (stress ranging from 0 to 210 MPa). Under no applied load, the voltage across the two wires was near zero and it increased to ~3 mV as the applied stress was increased to 195 MPa. The wire under (tensile) stress became cathodic (positive). Similarly, the current (when shorted externally) varied between zero and ~2 nA when the applied tensile stress was varied between zero and ~210 MPa. In both experiments as soon as the applied load was changed, the voltage/current changed sharply and equilibrated almost instantaneously. Fig. 4 shows the variation of the current between the stressed and the unstressed platinum foils as a function of time for different applied loads. The figure shows a discontinuity in the plot which is due to a temporary failure of the recording software. The higher measured current (as high as 170 nA) in the platinum foil experiment is attributed to the larger effective area of the foils as compared to the wires. It is also possible that the exchange current density on the wire surfaces may have been different than on foil surfaces due to possible differences in surface features/characteristics. Note that in this experiment also the current stabilized instantaneously and remained stable for the duration over which the stress was maintained constant.

Fig. 5 shows plots of the measured voltage across the wires as a function of the applied tensile stress for various wire diameters. In each case, the measured voltage varies linearly with the applied stress. However, the voltage difference, $\Delta\varphi$, at a given stress is higher for wires of larger diameters. This observation can be explained on the basis of the linear elasticity theory [54]. For an elastic body under stress, the three principal stresses in the Cartesian system are σ_{xx}, σ_{yy} and σ_{zz}. The corresponding hydrostatic pressure is given by [54]

$$p = -\frac{\sigma_{xx} + \sigma_{yy} + \sigma_{zz}}{3} \tag{11}$$

The corresponding principal strains are related to principal stresses by [54]

$$\varepsilon_{zz} = \frac{\sigma_{zz}}{E} - \frac{\nu}{E}(\sigma_{xx} + \sigma_{yy}) \tag{12}$$

$$\varepsilon_{xx} = \frac{\sigma_{xx}}{E} - \frac{\nu}{E}(\sigma_{yy} + \sigma_{zz}) \tag{13}$$

and

$$\varepsilon_{yy} = \frac{\sigma_{yy}}{E} - \frac{\nu}{E}(\sigma_{xx} + \sigma_{zz}) \tag{14}$$

where ν is the Poisson's ratio and E is the Young's modulus of elasticity. The two limiting cases in elasticity are of plane strain and plane stress [54]. Let us consider the application of a uniaxial load along the z direction. The corresponding stress is

$$\sigma_{zz} = \sigma \tag{15}$$

If plane strain conditions prevail,

$$\varepsilon_{yy} = \varepsilon_{xx} = 0 \quad \text{and} \quad \sigma_{yy} = \sigma_{xx} \tag{16}$$

Thus,

$$\varepsilon_{yy} = \varepsilon_{xx} = 0 = \frac{\sigma_{xx}}{E} - \frac{\nu}{E}(\sigma_{yy} + \sigma) = \frac{\sigma_{xx}}{E} - \frac{\nu}{E}(\sigma_{xx} + \sigma) \tag{17}$$

which gives [54]

$$\sigma_{xx} = \sigma_{yy} = \frac{\nu\sigma}{1-\nu} \tag{18}$$

Substituting Eqs. (15) and (18) into Eq. (11) and rearranging, the hydrostatic pressure is given by [54]

$$p = -\left(\frac{1+\nu}{1-\nu}\right)\frac{\sigma}{3} \tag{19}$$

If plane stress conditions are assumed, however, $\sigma_{yy} = \sigma_{xx} = 0$, and the corresponding hydrostatic pressure in the wire is given by [54]

$$p = -\frac{\sigma}{3} \tag{20}$$

It is well known in the theory of elasticity that for very thin foils/wires, plane stress conditions prevail, and for very thick

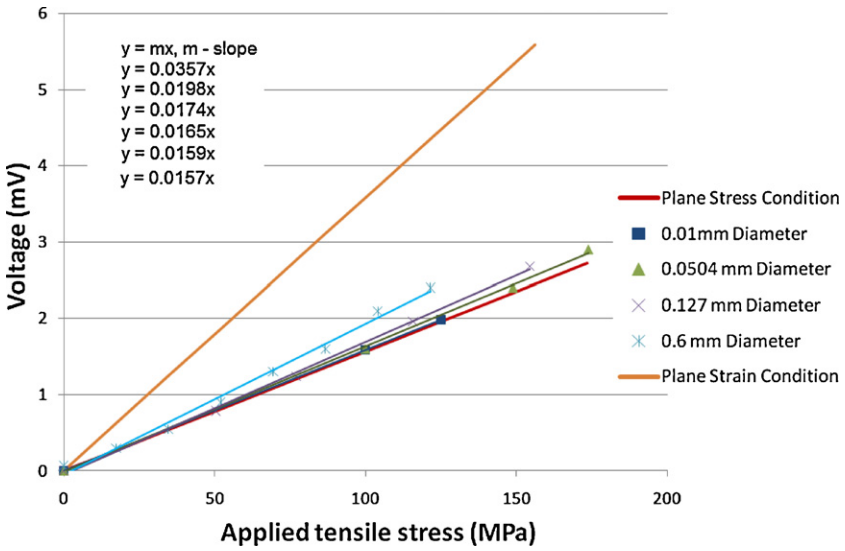

Fig. 5. Voltage between the stressed (positive) and the unstressed wires as a function of the applied tensile stress for varying wire diameters. The intercept is ideally zero. In the fitting of the experimental data, the very small nonzero intercept was neglected in the voltage vs. stress equations given in the inset. Slopes give voltage coefficients per unit stress.

plates/rods, plane strain conditions prevail [54]. From Eqs. (10) and (20), the difference in voltage between the stressed and the unstressed wires/foils under plane stress is given by

$$\frac{\mu^{o}_{Pt} - \mu_{Pt}}{2F} = \varphi(\sigma) - \varphi(0) = \Delta\varphi = \frac{V_m}{2F}\frac{\sigma}{3} = \frac{V_m}{6F}\sigma \quad (21)$$

where $\Delta\varphi$ is the voltage developed between the stressed and the unstressed wires/foils. Here platinum ions are assumed to be in +2 oxidation state even when the salt used was $PtCl_4$ since locally a reaction between $PtCl_4$ and Pt is expected to form Pt^{2+}. The theoretically calculated slope of $\Delta\varphi$ vs. σ from Eq. (21) is 1.57×10^{-11} V Pa^{-1}. For very thick wires, the prevailing state of stress will be that corresponding to plane strain. In such a case, the measured voltage will be given by

$$\varphi(\sigma) - \varphi(0) = \Delta\varphi = \frac{V_m}{2F}\frac{(1+\nu)\sigma}{(1-\nu)3} = \frac{V_m}{6F}\left(\frac{1+\nu}{1-\nu}\right)\sigma \quad (22)$$

For Pt, the Poisson's ratio is $\nu \approx 0.39$. The estimated slope for plane strain from Eq. (22) is 3.57×10^{-11} V Pa^{-1}. The measured slopes of the plots in Fig. 5 range between $\sim 1.59 \times 10^{-11}$ V Pa^{-1} for a 10 micron wire diameter, which is close to the plane stress case, and $\sim 1.98 \times 10^{-11}$ V Pa^{-1} for a 0.6 mm wire diameter. Fig. 6 shows

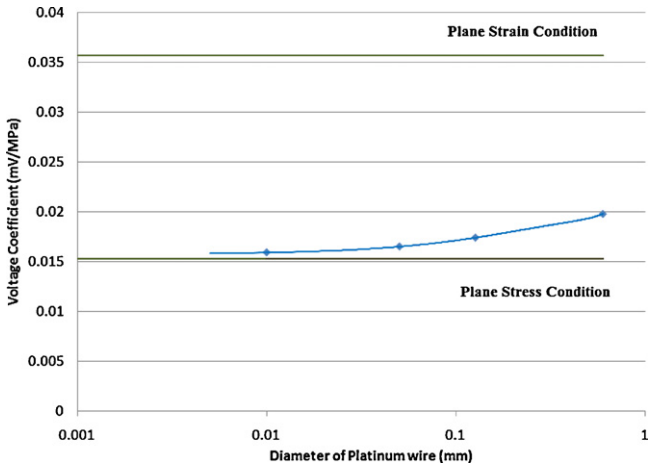

Fig. 6. Variation of the voltage coeffient per unit stress as a function of the diameter of platinum wire.

the variation of the measured slopes or voltage coefficients per unit stress as a function of the wire diameter. The increase in slope with increasing diameter is in accord with the predictions of the linear elasticity theory. The present results also show that a wire diameter of 0.6 mm is far below that required for plane strain conditions to prevail. It will be necessary to use rods of much larger diameters to reach plane strain conditions. This was beyond the practical range of the current experiments.

The present results also show that the dominant electrode reactions are $Pt \rightarrow Pt^{2+} + 2e'$ (anodic) at the unstressed wire/foil and $Pt^{2+} + 2e' \rightarrow Pt$ (cathodic) at the (tensile) stressed wire/foil even though the salt was $PtCl_4$. If the dominant reactions had been $Pt \rightarrow Pt^{4+} + 4e'$ and $Pt^{4+} + 4e' \rightarrow Pt$, the measured $\Delta\varphi$ would have been

$$\Delta\varphi = \frac{V_m}{12F}\sigma \quad (23)$$

or half the observed values. If both reactions had occurred to comparable extents, the magnitude of the measured potential, $\Delta\varphi$, would have been between the values given by Eqs. (23) and (21), resulting in mixed potential. The observation that the measurements are in agreement with Eq. (21) suggests that the present results were not influenced by any mixed potential effects.

4.2. SEM observations of wires and foils

Fig. 7(a) and (b) respectively shows SEM micrographs of the unstressed and stressed platinum wires (externally shorted) after 144 h of treatment in 0.1 M $PtCl_4$/DMSO solution. The diameter of the unstressed platinum wire immersed in the solution shrank from 127 μm to 122 μm and that of the stressed wire increased from 127 μm to 134 μm. Fig. 7(b) shows part of the stressed wire that was not immersed in the electrolyte; it exhibited no change in diameter. Fig. 8(a) and (b) respectively show SEM micrographs of the cross sections of the unstressed and the stressed platinum foils (externally shorted) after 144 h of treatment in 0.1 M $PtCl_4$/DMSO solution. The thickness of the unstressed foil shrank from 127 μm to 116 μm and that of the stressed foil increased from 127 μm to about 138 μm. Fig. 8(a) shows the interface region where the top portion of the unstressed foil was outside the electrolyte and the bottom portion was immersed in the electrolyte. The volume of platinum deposited on the stressed wire/foil will be the same as the volume of

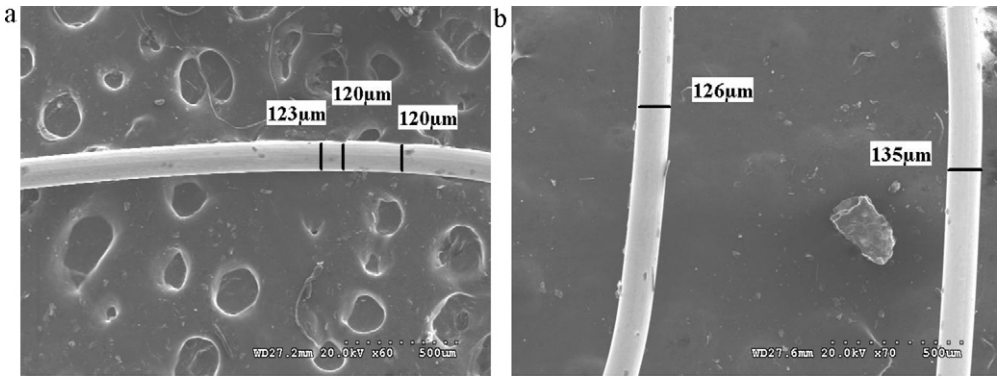

Fig. 7. SEM micrographs of: (a) unstressed platinum wire immersed in 0.1 M $PtCl_4$/DMSO electrolyte for 144 h. The wire diameter shrank to ~120 μm. (b) Stressed platinum wire: the portion of platinum wire outside the electrolyte (no growth) – 126 μm, and stressed platinum wire immersed in electrolyte – 135 μm (wire diameter increased to 135 μm).

platinum dissolved at the unstressed wire/foil. In the experimental data, it seemed that the decrease in the unstressed wire diameter is less than the increase in the diameter of the stressed wire. Since the volume of Pt is conserved, this observation is attributed to the fact that the lengths of the wires immersed in the solution were not the same for the two wires (the unstressed wire was a bit curled and thus a little longer than the stressed one in the immersed state).

4.3. The sign of stress/potential and chemical potential

According to Eq. (21) the application of a tensile load/stress (leading to negative pressure) to a platinum wire/foil lowers the chemical potential of Pt compared to the unstressed wire/foil. In some of the literature, it has been often assumed that applied stress always increases the chemical potential through the strain energy term [55]. This, however, is incorrect. Excellent discussion of this point has been given by Flood several decades ago [52]. The analysis by Flood [52] is in agreement with the original analysis by Gibbs which has often been ignored in some recent literature [55]. Also, experiments conducted on pure metals over 60 years ago are in accord with Flood's analysis [50,51] and in accord with the predictions of thermodynamics. Thus, platinum ions tend to move from higher chemical potential of neutral Pt or Pt^{2+} (unstressed wire/foil) to lower chemical potential of neutral Pt or Pt^{2+} (wire/foil under a tensile stress). As the electron concentration is negligible in the electrolyte, transport of Pt^{2+} shuts down when the electrochemical potential of Pt^{2+} becomes equal in both wires. The wire subjected to a tensile stress develops a positive potential (becomes cathodic) with respect to the unstressed wire. The equilibrium electric potential difference corresponds to the difference in chemical potentials of Pt and is given by Eq. (21) for plane stress (thin wire/foil) or Eq. (22) for plane strain (thick wire/foil). When an external path is provided for electrons by shorting the wires/foils, the circuit is completed; Pt ions move from the unstressed wire/foil to the stressed (tensile) wire/foil through the electrolyte and electrons transport from the unstressed to the stressed (tensile) wire/foil in the external circuit. In this manner, net transport of neutral Pt occurs from the unstressed wire/foil to the stressed (tensile) wire/foil. This results in the thickening of the stressed (tensile) wire/foil and shrinking of the unstressed wire/foil, as observed in the present experiments. If the wire/foil had been stressed compressively (it would be more convenient to use a bar instead of wire/foil to prevent buckling), then the sign of the voltage developed would have been opposite; the compressively stressed one would have been negative (anodic). When connected externally, Pt transport would occur from the compressively stressed to the unstressed wire/foil.

5. Implications concerning core–shell catalysts for PEMFC

In PEMFC electrodes catalyst particles are supported on an electronically conducting carbon support, which provides an electronic path. Particle growth occurs by a coupled transport of Pt ions through the liquid/ionomer and of electrons through the carbon support [48]. The present results and the preceding discussion suggest an approach for the synthesis of durable core–shell catalysts.

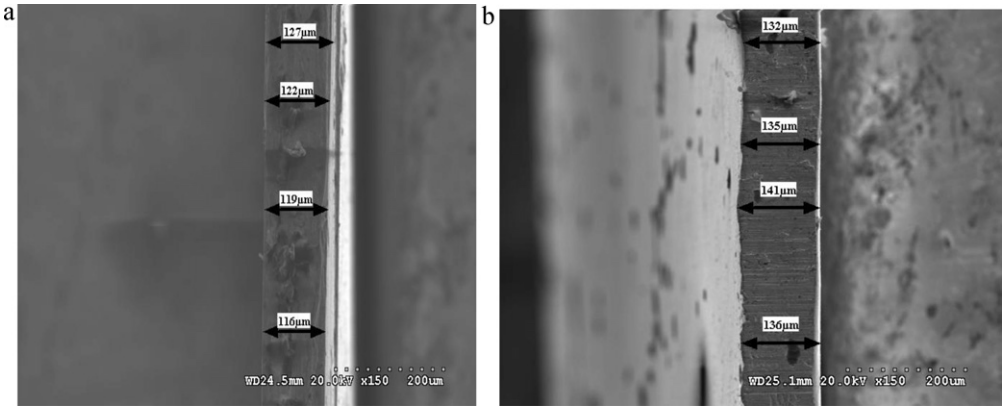

Fig. 8. SEM micrographs of foils immersed in 0.1 M $PtCl_4$/DMSO electrolyte for 144 h. (a) Cross-section of the interface of the unstressed platinum foil where the top portion of the foil was outside the electrolyte (no change) and the bottom portion was immersed in the electrolyte (where dissolution occurred). The thickness reduced to ~116 μm. (b) Cross-section of stressed platinum foil immersed in the electrolyte. The thickness increased to ~136 μm.

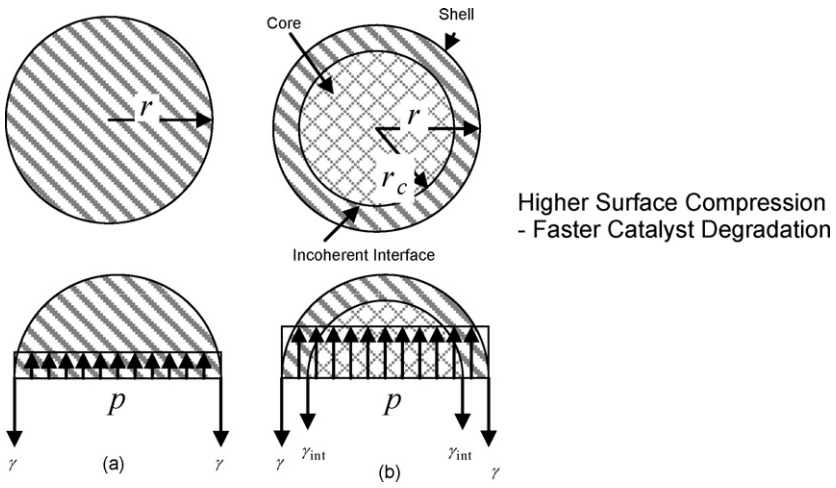

Fig. 9. Schematics of (a) monolithic and (b) core-shell catalyst with an incoherent interface. Compressive stress in the shell is higher than the compressive stress in a monolithic catalyst particle. Such a catalyst should be less stable against dissolution compared to the monolithic particle.

Much of the reported work on core–shell catalysts has been primarily conducted with the objective of decreasing the Pt loading and also enhancing the catalyst activity [1,9,12,13]. While stability is well recognized as an important consideration, clear design strategies had not been defined. Many recent studies have addressed stability of core–shell catalysts [16–19,22,25,28,34]. The majority of the studies are either (out-of-cell) experimental in which catalyst performance is investigated using cyclic voltammetry or theoretical in which stability is inferred on the basis of DFT calculations [34]. The present results suggest that if a tensile stress (or reduced compression) exists in the Pt shell as compared to a pure Pt particle, its chemical potential will be lowered and its stability against dissolution will be increased. In many core–shell catalyst studies, the nature of the core–shell interface has not been discussed in the literature. For example, in some studies the Pt shell was deposited on a core of a material of a different crystal structure leading to an incoherent interface. Fig. 9 compares a monolithic Pt catalyst with a core–shell catalyst having an incoherent interface. In such a case, the compressive stress in the Pt shell will be higher than in a monolithic Pt catalyst. The pressure in the shell is given by

$$p = \frac{2\gamma}{r} + \frac{2\gamma_{\text{int}} r_c}{r^2} \tag{24}$$

where r_c is the core radius, r is the outer radius and γ_{int} is the interfacial energy between the core and the shell. If, however, the core–shell interface is perfectly coherent, γ_{int} is negligible, and if the lattice parameter of the core is larger than the Pt shell, such as with Ag or Au core, the corresponding comparison between a monolithic Pt particle and a core–shell catalyst is shown in Fig. 10. The corresponding state of stress in the shell is given by

$$p(r) = \left(\frac{2\gamma}{r} - \frac{2\sigma_{\theta\theta}}{3}\right) \tag{25}$$

where $\sigma_{\theta\theta} = \sigma_{\phi\phi}$ are principal (angular, using a spherical polar coordinate system) stresses in the shell caused by the lattice mismatch between the shell and the core [54]. At the surface, the state of stress is symmetric bi-axial (with the radial stress, σ_{rr}, on the surface of the shell being zero). The corresponding chemical potential of Pt in the shell is

$$\mu_{\text{Pt}}(r) = \mu^{\circ}_{\text{Pt}} + \left(\frac{2\gamma}{r} - \frac{2\sigma_{\theta\theta}}{3}\right) V_m \tag{26}$$

Note that if tensile stresses are created in the shell due to lattice parameter mismatch, we have $\sigma_{\theta\theta} = \sigma_{\phi\phi} > 0$. In such a case, the chemical potential of Pt in the shell of such a core shell catalyst will be lower than the corresponding monolithic Pt catalyst particle of the same radius. The difference in chemical potentials between the shell of a core–shell catalyst and a monolithic Pt catalyst is given by

$$\Delta\mu_{\text{Pt}}(r) = -\left(\frac{2\sigma_{\theta\theta}}{3}\right) V_m \tag{27}$$

If the core and the shell are of the same crystal structure, a coherent interface between the core and the shell is expected (assuming lattice parameter mismatch is not too large and the shell is thin). Pt is f.c.c. (A1 structure). Other metals belonging to the same structure are Ag, Au, Cu, Pd, Ni, Co (when existing as small particles), etc. Lattice parameters of Cu, Ni, Co are smaller than that of Pt. Thus, core–shell catalysts made with these metals as the core will have the Pt shell in additional compression due to the lattice mismatch. This compressive stress will be in addition to the $2\gamma/r$ pressure created by the surface energy term (Gibbs–Thompson effect). The prediction thus is that core–shell catalysts made with Cu or Ni or Co as core will tend to be less stable compared to pure Pt catalyst. If, however, core–shell catalysts are made with Ag or Au as the core which have larger lattice parameters than Pt, the Pt shell will be under a tensile stress (or reduced compression). Such core–shell catalysts will be more stable against dissolution compared to monolithic Pt catalysts (Fig. 10).

The magnitude of the tensile stress in the Pt shell depends upon the difference in the lattice parameters, the elastic properties and particle/shell dimensions. The lattice parameter of Pt is 0.3923 nm and that of Ag is 0.40863 nm. The corresponding strain in a thin shell of the Ag core–Pt shell catalyst is on the order of ~4%. The Young's modulus of Pt is 168 GPa. A hydrostatic tensile stress on the order of ~4 GPa can be expected in the shell of Pt. Such a high stress is possible if the interface is perfectly coherent with no dislocations present. The corresponding EMF is given by $\Delta\varphi = (\sigma_h V_m)/(2F)$ or ~190 mV as compared to a monolithic Pt catalyst. This means cathodic protection of Ag core–Pt shell catalysts by ~190 mV compared to monolithic Pt catalysts. This is a very significant effect. It implies that the stability of the Pt-shell Ag-core (Ag@Pt) catalyst may be enhanced by ~190 mV in comparison to monolithic Pt catalysts. Thus, core–shell catalysts with Ag as the core will lower the chemical potential of Pt in the shell. Therefore, the prediction is that Ag-core–Pt-shell (Ag@Pt) catalysts will be more stable than pure Pt catalysts. Preliminary experiments have in fact shown that Ag/Pt core–shell (Ag@Pt) catalysts are more stable than pure Pt catalysts [56].

Recently, Ramirez-Caballero et al. [34] conducted detailed DFT calculations of core–shell catalysts. In their work relative stability

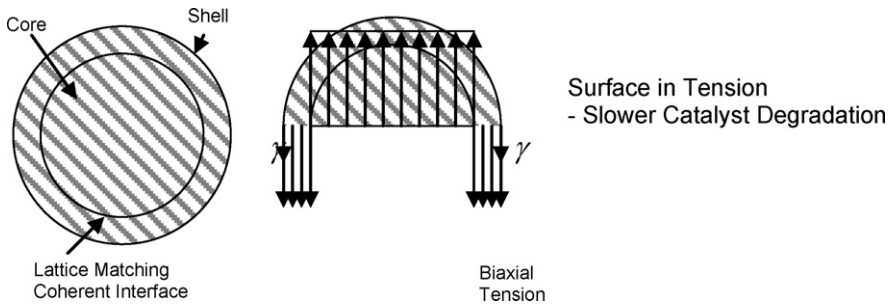

Fig. 10. Schematic of a core-shell catalyst with a coherent interface. Compressive stress in the shell is lower than the compressive stress in a monolithic particle. Such a catalyst should be more stable against dissolution compared to the monolithic particle.

Table 1
Comparison of the estimates of relative stability (+)/instability (−) of core–shell catalysts based on the DFT calculations of Ramirez-Caballero et al. [34] and the present results based on a thermodynamic analysis.

Core/(Pt) shell catalyst	DFT calculations of Ramirez Caballero et al. [34] Relative stability (+) Instability (−) of Pt shell In volts	Present results based on a thermodynamic analysis Relative stability (+) Instability (−) of Pt shell In volts
Ag@Pt	+0.20	+0.19
Au@Pt	+0.16	+0.18
Co@Pt	−0.59	−0.50
Ni@Pt	−0.60	−0.52
Cu@Pt	−0.084	−0.40
Pd@Pt	+0.15	−0.04

of core–shell catalysts was investigated. In DFT calculations, the possible effects of stress are not separately accounted for. However, the energy minimization schemes used in such calculations include all effects, including the effect of stress. Ramirez-Caballero et al. [34] estimated that Pt-shell/Ag-core (Ag@Pt) catalysts should increase the stability of core–shell catalysts by ∼200 mV. Thus, these DFT calculations [34] and the results of continuum modeling based on thermodynamics presented here are in very good agreement.

The lattice parameters of Au, Co, Ni, and Cu are respectively, 0.40786 nm, 0.3544 nm, 0.35239 nm, and 0.36148 nm. Similar calculations as above give $\Delta\varphi = (\sigma_h V_m)/(2F)$ of ∼180 mV, ∼−500 mV, ∼−520 mV, and ∼−400 mV, respectively. That is, according to the present calculations, stability of Au@Pt will be enhanced by ∼180 mV with respect to monolithic Pt catalysts. However, stability of Co@Pt, Ni@Pt and Cu@Pt will be decreased by ∼500 mV, ∼520 mV, and ∼400 mV, respectively. DFT calculations of Ramirez-Caballero et al. [34] show that for Au@Pt the stability is increased by ∼160 mV. By contrast, stabilities of Co@Pt, Ni@Pt, and Cu@Pt will be decreased by ∼590 mV, ∼600 mV, and ∼84 mV, respectively. With the exception of the Cu@Pt, the results of present calculations based on a thermodynamic analysis are in good agreement with the DFT calculations of Ramirez-Caballero et al. [34]. Also, DFT calculations show Pd@Pt should be more resistant to dissolution than monolithic Pt catalysts. Since the lattice parameters of Pd and Pt are about the same (Pd is slightly smaller), the present work, by contrast, predicts little effect of stress in Pd@Pt. However, it is to be noted that the thermodynamic analysis presented here can only address the effect of stress. It cannot address possible chemical/electronic interactions between the shell and the core, for example the shift of the d-band center, which are included in the DFT calculations [34]. Thus, differences in Cu@Pt and Pd@Pt may well be related to electronic/chemical effects as discussed by Ramirez-Caballero et al. [34]. The comparison between the present work and the results of Ramirez-Caballero et al. [34] nevertheless shows that probably the stress effect is more dominant. The results of these estimates are also listed in Table 1. These results also show that thermodynamic analysis based on continuum modeling is useful for the design of materials and catalysts in the nanoscale range.

Recent work by Sasaki et al. [57] has shown that Pd@Pt catalysts undergo leaching of Pd-core. These authors have reported stable Pd-core catalysts with monolayer Pt shell. It is to be noted, however, that studies by Sasaki were conducted for relatively short periods of time (albeit several thousands of cycles). For long term applications in the actual PEMFC, it is equally or more important to conduct tests for thousands of hours. No such information on Pd@Pt is currently available. Thus, long term stability of Pd@Pt in actual fuel cells under realistic operating conditions still remains to be demonstrated.

In the present work, a simple relation for the pressure generated due to surface energy, $2\gamma/r$, was assumed for nanosize particles. Many recent studies have used equations of state which incorporate crystallographic orientation dependence of surface energies. This may be especially important for very small atom clusters, which display various shapes depending upon the number of atoms in the cluster [58–60]. However, there also are numerous studies on nanosize particles which assume an isotropic surface energy. This simple assumption is found to be quite reasonable for particles 2 nm and larger as evidenced by their often observed near spherical shape, typical of PEMFC catalysts. A more refined estimate, while still assuming isotropic surface energy, is the inclusion of the size dependence of the surface energy itself. For example, several studies have shown that for very small particles, γ itself is a function of the particle size, r, that is $\gamma(r)$ [61–64]. Then the pressure created by the surface energy term is $2\gamma(r)/r$.

6. Summary

The effect of applied stress on the chemical potential of Pt was measured using an electrochemical cell. Two platinum wires/foils were immersed in a $PtCl_4$/DMSO solution. One of the wires/foils was subjected to a tensile stress while the other one was left load free. It was observed that the wire/foil subjected to a tensile stress developed a positive electric potential compared to the unstressed one, indicating that the application of a tensile stress decreases the chemical potential of platinum. This result is in accord with the thermodynamic theory of Gibbs and the analy-

sis given by Flood [52]. The measured voltage coefficient per unit stress increased with increasing wire diameter. For wires of the smallest diameter used, the voltage coefficient per unit stress corresponded to the state of plane stress. The voltage developed per unit stress increased with increasing wire diameter. Increasing voltage coefficient per unit stress with increasing diameter is in accord with the predictions of linear elasticity that a transition from plane stress to plane strain should occur when using rods of sufficiently large diameters. When the wires/foils were connected externally, the diameter/thickness of the one under tensile stress grew while the diameter/thickness of the unstressed one shrank.

These results suggest an approach for the development of stable cathode catalysts for PEMFC [65]. The present work shows that core–shell catalysts consisting of a core and a Pt shell having the same crystal structures, the Pt shell having a smaller lattice parameter than the core, and the Pt shell epitaxially matched to the core will result in a tensile stress (or reduced compression) in the Pt shell. Such core–shell catalysts should be inherently more stable as the tensile stress in the Pt shell will lower its chemical potential and decrease its tendency for dissolution. The predictions of the stability of Ag@Pt core–shell catalysts based on the effect of tensile stress in the shell in the present work are consistent with DFT calculations reported in the literature [34]. Both the DFT calculations [34] and the present thermodynamic analysis predict a stability of Ag@Pt against dissolution by about ~190–200 mV. The present work thus also demonstrates the utility of continuum thermodynamic modeling in the design of nanoscale materials.

Acknowledgement

This work was supported by the National Science Foundation under Grant Number CBET-0931080.

References

[1] Y. Xu, A.V. Ruban, M. Mavrikakis, J. Am. Chem. Soc. 126 (14) (2004) 4717–4725.
[2] R. Srivastava, P. mani, N. Hanh, P. Strasser, Angew. Chem. Int. Ed. 46 (47) (2007) 8988–8991.
[3] T. Toda, H. Igarashi, M. Watnabe, J. Electroanal. Chem. 460 (1–2) (1999) 258–262.
[4] S. Mukerjee, S. Srinivasan, M.P. Soriaga, J. McBreen, J. Electrochem. Soc. 142 (5) (1995) 1409–1422.
[5] K. Kinoshita, Electrochemical Oxygen Technology , Wiley, New York, 1992, pp. 133–140.
[6] V. Jalan, E.J. Taylor, J. Electrochem. Soc. 130 (11) (1983) 2299–2300.
[7] U. Koponen, H. Kumpulainen, M. Bergelin, J. Keskinen, T. Peltonen, M. Valkianen, M. Wasberg, J. Power Sources 118 (1–2) (2003) 325–333.
[8] B. Gurau, R. Viswanathan, R. Liu, T.J. Lafrenz, K.L. Ley, E.S. Smotkin, E. Reddington, A. Sapienza, B.C. Chan, T.E. Mallouk, S. Sarangpani, J. Phys. Chem. B 102 (49) (1998) 9997–10003.
[9] J. Zhang, F. Lima, M. Shao, K. Sasaki, J. Wang, J. Hanson, R. Adzic, J. Phys. Chem. B 109 (2005) 22701–22704.
[10] J. Zhai, M. Huang, S. Dong, Electroanalysis 19 (4) (2007) 506–509.
[11] S. Yamamoto, Electrode Catalyst for fuel cell and method for production thereof. US Patent 7,205,255 (date of Issue: April 17, 2007).
[12] W. Zhou, J.Y. Lee, Electrochem. Commun. 9 (7) (2007) 1725–1729.
[13] P. Strasser, Platinum-rich shell, platinum poor core. Public release date: October 23, 2007, http://www.rsc.org/chemistryworld/News/2007/October/30100701.asp.
[14] Z.D. Wei, Y.C. Feng, L. Li, M.J. Liao, Y. Fu, C.X. Sun, Z.G. Shao, P.K. Shen, J. Power Sources 180 (2008) 84–91.
[15] S. Ball, S.L. Burton, E. Christian, A. Davies, R. O'Malley, S. Passot, B. Tessier, B.R.C. Theobald, D. Thompsett, ECS Trans. 25 (1) (2009) 1011–1022.
[16] R.R. Adzic, J. Zhang, K. Sasaki, M.B. Vukmirovic, M. Shao, J.X. Wang, A.U. Nilekar, M. Mavrikakis, J.A. Valerio, F. Uribe, Top Catal. 46 (2007) 249–262.
[17] W. Zhou, J.Y. Lee, Electrochem. Commun. 9 (2007) 1725–1729.
[18] B. Fang, B.N. Wanjala, X. Hu, J. last, R. Loukrapam, J. Yin, J. Luo, C.-J. Zhong, J. Power Sources 196 (2011) 659–665.
[19] P. Hirunsit, P.B. Balbuena, J. Phys. Chem. C 114 (2010) 13055–13060.
[20] J.K. Norskov, T. Bligaard, J. Rossmeisl, C.H. Christensen, Nat. Chem. 1 (April (37)) (2009).
[21] J. Zhai, M. Huang, S. Dong, Electroanalysis 19 (2007) 506–509.
[22] Y. Ma, P.B. Balbuena, J. Electrochem. Soc. 157 (6) (2010) B959–B963.
[23] S. Zhou, G.S. Jackson, B. Eichhorn, Adv. Funct. Mater. 17 (2007) 3099–3104.
[24] Z. Peng, H. Yang, Nano Res. 2 (2009) 406–415.
[25] Y. Xing, Y. Cai, M.B. Vukmirovic, W.-P. Zhou, H. Karan, J.X. Wang, R.A. Adzic, J. Phys. Chem. Lett. 1 (2010) 3238–3242.
[26] Y. Chen, F. Yang, Y. Dai, W. Wang, S. Chen, J. Phys. Chem. C 112 (2008) 1645–1649.
[27] Z. Yang, J.Y. Yang, Q. Zhang, W. Zhou, Z. Liu, J. Electrochem. Soc. 155 (7) (2008) B776–B781.
[28] R. Srivastava, P. Mani, N. Hahn, P. Strasser (Eds.), Angew. Chem. Int. 46 (2007) 8988–8991.
[29] Y. Ma, H. Zhang, H. Zhing, T. Xu, H. Jin, X. Geng, Catal. Commun. 11 (2010) 434–437.
[30] B.C. Tessier, A.E. Russell, B. Theobald, D. Thompsett, ECS Trans. 16 (37) (2009) 1–11.
[31] P.P. Wells, E.M. Crabb, C.R. King, R. Wiltshire, B. Billsborrow, D. Thompsett, A.E. Russell, Phys. Chem. Chem. Phys. 11 (2009) 5773–5781.
[32] Z. Liu, G.S. Jackson, B.W. Eichhorn, Angew. Chem. 122 (2010) 3241–3244.
[33] S. Koh, J. Leisch, M.F. Toney, P. Strasser, J. Phys. Chem. C 111 (2007) 3744–3752.
[34] G.E. Ramirez-Caballero, Y. Ma, R. Callejas-Tovar, P.B. Balbuena, Phys. Chem. Chem. Phys. 12 (2010) 2209–2218.
[35] M.S. Wilson, F.H. Garzon, K.E. Sickhaus, S. Gottesfeld, J. Electrochem. Soc. 140 (10) (1993) 2872–2877.
[36] R. Ornelas, A. Stassi, E. Modica, A.S. Arico, V. Antonucci, ECS Trans. 3 (1) (2006) 633–641.
[37] X. Wang, R. Kumar, D. Meyers, J. Electrochem. Solid State Lett. 9 (5) (2006) A225–A227.
[38] J. Xie, D.L. Wood III, K.L. More, P. Atanassov, R.L. Borup, J. Electrochem. Soc. 152 (5) (2005) A1011–A1020.
[39] P.J. Ferreira, G.J. Lao, Y. Shao-Horn, D. Morgan, R. Makharia, S. Kocha, H.A. Gasteiger, J. Electrochem. Soc. 152 (11) (2005) A2256–A2271.
[40] W. Bi, G.E. Gray, T.F. Fuller, Electrochem. Solid State Lett. 10 (5) (2007) B101–B104.
[41] K. Yasuda, A. Taniguchi, T. Akita, Z. Siroma, Phys. Chem. Chem. Phys. 8 (746) (2006).
[42] A. Ohma, S. Suga, S. Yamamoto, K. Shinohara, in: T. Fuller, et al. (Eds.), Proton Exchange Membrane Fuel Cells 6, ECS Trans. 3 (1) (2006) 519–529.
[43] H. Liu, J. Zhang, F.D. Coms, W. Gu, B. Litteer, H.A. Gasteiger, in: T. Fuller, et al. (Eds.), Proton Exchange Membrane Fuel Cells 6, ECS Trans. 3 (1) (2006) 493–505.
[44] A. Laconti, H. Liu, C. Mittelsteadt, R. McDonald, in: T. Jarvi, et al. (Eds.) ECS Trans. 1 (8) (2005) 199–219.
[45] B. Merzougui, S. Swathirajan, J. Electrochem. Soc. 153 (12) (2006) A2220–A2226.
[46] K.L. More, R. Borup, K.S. Reeves, ECS Trans. 3 (1) (2006) 717–733.
[47] R. Darling, J. Meyers, J. Electrochem. Soc. 150 (11) (2003) A1523–A1527.
[48] A.V. Virkar, Y. Zhou, J. Electrochem. Soc. 154 (6) (2007) B540–B547.
[49] O.F. Devereux, Topics in Metallurgical Thermodynamics , John Wiley-Interscience, New York, 1983.
[50] R.E. Fryxell, N.H. Nachtrieb, J. Electrochem. Soc. 99 (495) (1952).
[51] S. Tan, K. Nobe, Can. J. Chem. 41 (1963) 495–498.
[52] E.A. Flood, Can J. Chem. 36 (1958) 1332–1337.
[53] I. Barin, Thermochemical Data of Pure Substances. Part II , VCH Publication, Weinheim, Germany, 1993.
[54] S.P. Timoshenko, J.N. Goodier, Theory of Elasticity , McGraw-Hill, New York, 1970.
[55] A. Horvath, R. Schiller, Phys. Chem. Chem. Phys. 3 (2001) 2662–2667.
[56] J.-H. Koh, R. Abbaraju, N. Dasgupta, A.V. Virkar, unpublished work, 2009.
[57] K. Sasaki, H. Naohara, Y. Cai, Y.M. Choi, P. Liu, M.B. Vukmirovic, J.X. Wang, R.R. Adzic, Angew. Chem. Int. Ed. 49 (2010) 8602–8607.
[58] R.V. Chepulski, S. Curtarolo, ACS Nano 5 (1) (2011) 247–254.
[59] S.-P. Huang, P.B. Balbuena, Mol. Phys. 100 (13) (2002) 2165–2174.
[60] X. Shao, X. Wu, W. Cai, J. Phys. Chem. A 114 (2010) 12813–12818.
[61] A.N. Goldstein, C.M. Echer, A.P. Alivisatos, Science 256 (1425) (1992).
[62] H. Hofmeister, S. Thiel, M. Dubiel, E. Schurig, Appl. Phys. Lett. 70 (1694) (1997).
[63] K.K. Nanda, A. Maisels, F.E. Kruis, H. Fissan, S. Stappert, Phys. Rev. Lett. 91 (10) (2003), 106102-1–106102-4.
[64] B. Medasani, Y.H. Park, I. Vasiliev, Phys. Rev. B 75 (2007) 23546.
[65] A.V. Virkar, Core–Shell Catalyst, US Patent Application No. 20,100,062,929 (filed 2008).